

Article

Investigations of the Mechanical Properties and Durability of Reactive Powder Concrete Containing Waste Fly Ash

Yubing Du ^{1,2}, Shiyu Wang ³, Wenru Hao ⁴, Feiting Shi ¹, Hui Wang ⁵, Feng Xu ⁵ and Tao Du ^{6,*}

- ¹ College of Civil Engineering, Yancheng Institute of Technology, Yancheng 224051, China; duyubing@ycit.cn (Y.D.); shifeiting@ycit.cn (F.S.)
 - ² College of Civil Aviation, Nanjing University of Aeronautics and Astronautics, Nanjing 210016, China
 - ³ Shanghai Jianke Group Co., Ltd., Shanghai 200020, China; wangshiyu@sribs.com
 - ⁴ School of Civil and Transportation Engineering, Beijing University of Civil Engineering and Architecture, Beijing 102616, China; haowenru1@163.com
 - ⁵ School of Civil and Environmental Engineering, Ningbo University, Ningbo 315000, China; huiwang123@aliyun.com (H.W.); xufeng@163.com (F.X.)
 - ⁶ School of Mechanics and Civil Engineering, China University of Mining and Technology, Xuzhou 221000, China
- * Correspondence: dutao@cumt.edu.cn

Abstract: Waste fly ash (WFA) with pozzolanic activities may be advantageous to the mechanical properties of reactive powder concrete (RPC) when WFA partially replaces cement in RPC. In this study, RPC specimens with 0–25% WFA were prepared under the curing temperatures of 0, 20, and 40 °C for 3 to 120 days. The flowability of fresh RPC, the mechanical strengths, and the NaCl freeze–thaw damage were investigated. Additionally, the following carbonation depths after different NaCl freeze–thaw cycles and the leaching amount of toxic metal elements were also determined experimentally. The results indicated that the incorporation of WFA could decrease the slump flow of fresh RPC due to the relatively smaller particle size of WFA. With an increase in the WFA content, the early-age flexural and compressive strengths first exhibited an increasing and then decreasing trend. However, WFA will always deteriorate the long-term mechanical properties, and both flexural and compressive strengths can be reduced by up to 25% when cured for 120 days. A higher temperature (i.e., 40 °C) was found to benefit the mechanical properties, especially when cured for 3 days. The RPC with 10% WFA exhibited the optimum salt-freezing resistance with an approximately 30% reduction in the mass loss rate when the NaCl freeze–thaw cycles reached 300. The improvement in durability can be attributed to a more compact microstructure of RPC with WFA through microscopic observations. The relationships between the mass and mechanical strength loss rates can be expressed through positive correlation quadratic functions. The carbonation depth decreased following a quadratic function with increasing mass ratios of WFA and NaCl freeze–thaw cycles. The leaching amounts of Cr and Zn increased with increasing WFA content over time, and the cumulative values reached equilibrium at 5 months.

Keywords: waste fly ash; reactive powder concrete; carbonation; toxic metal elements; NaCl freeze–thaw cycles

Citation: Du, Y.; Hao, W.; Shi, F.; Wang, H.; Xu, F.; Du, T. Investigations of the Mechanical Properties and Durability of Reactive Powder Concrete Containing Waste Fly Ash. *Buildings* **2022**, *12*, 560. <https://doi.org/10.3390/buildings12050560>

Academic Editors: Elhem Ghorbel and Elena Ferretti

Received: 23 February 2022

Accepted: 25 April 2022

Published: 27 April 2022

Publisher's Note: MDPI stays neutral with regard to jurisdictional claims in published maps and institutional affiliations.



Copyright: © 2022 by the authors. Licensee MDPI, Basel, Switzerland. This article is an open access article distributed under the terms and conditions of the Creative Commons Attribution (CC BY) license (<https://creativecommons.org/licenses/by/4.0/>).

1. Introduction

Municipal solid waste incineration (MSWI) fly ash is domestic waste burned at high temperature. The waste fly ash (WFA) contains the heavy metals Zn, Cr, Pb, and Cd with high leaching concentration and dioxin with high toxic equivalent, which belongs to hazardous solid waste [1,2]. The environmental protection department requires that the toxic ions in WFA must be solidified and undergo stabilizing treatment. Currently, the main

treatment methods of fly ash in various countries include direct landfill after cement solidification and stabilization. These disposal methods waste large amounts of land resources and disposal costs. Harmful heavy metals and dioxins in fly ash easily penetrate into soil and groundwater, resulting in secondary pollution [3].

Besides the hazardous constituents, the main chemical compositions of fly ash are similar to those of cement clinker including silica (SiO_2), lime (CaO), alumina (Al_2O_3), and iron oxide (Fe_2O_3) [4]. These compositional features enable the application of fly ash in cement-based materials. Meanwhile, with the increasing shortage and depletion of resources for use in human construction, the application of solid waste production in cement concrete may become an inevitable development trend in the concrete industry [5]. Fly ash has been investigated as a substitute for raw materials in cement production [6], and it has also been blended in cement as supplementary cementitious material (SCM) [7]. However, the chemical composition of fly ash is highly dependent on its diverse sources, which makes it challenging for use in the production of cement. In addition, the high-temperature sintering process of cement production increases the risk of releasing pollutants from fly ash [8]. Given the pozzolanic properties of fly ash, more attempts have been made in the application of fly ash as a cement replacement in the production of concrete [9].

The properties of cement-based materials blended with fly ash have been extensively studied. Polettini et al. [10] pointed out that both the heavy metals and alkalis from fly ash play important roles in influencing the setting and hardening process of cement. Due to the high porosity of MSWI ashes, the water demand of blended cement is found to be higher than typical Portland cement [11]. Meanwhile, the setting times of cement with MSWI ashes are longer owing to a reduced hydration rate [12]. Li et al. [13] also reported that MSWI bottom ash will hinder cement hydration due to the low cementitious activity. Rehman prepared a 3D printable concrete by mixing MSWI ash and found that the MSWI ash can partially replace cement without violating the rheological requirements of 3D printed concrete [14]. Alderete investigated the fresh and hardened properties as well as the durability properties of concrete with municipal solid waste ash as part of a cement substitute; it indicated that a well-performing concrete mix can be designed when using municipal solid waste ash as 20% of the binder [15]. Tang et al. [16] pointed out that the compressive and flexural strengths of cement mortar decreased by 16% and 6% when 30% cement was replaced by thermally activated MSWI bottom ash. Bertolini et al. [17] found that both the strength and durability of concrete were negatively affected by incorporating dry-grounded MSWI bottom ash, which was attributed to the entrapment of gas bubbles induced by cathodic reaction. Although, some studies on the mechanical strengths, durability, and microstructures of cement-based materials were reported, little attention has been paid to the coupling effects of multiple groups of environmental factors on the variation in the performances of cement-based materials with MSWI ash when this kind of cement concrete is applied in a coastal environment. Furthermore, the leaching properties of fly ash in cement paste was investigated by Shi et al. [18], who indicated that the leaching of heavy ions mainly occurs at early ages. Moreover, it was reported that the curing temperature is a key factor in the strength development of fly-ash-based geopolymer [19]. Therefore, the curing temperature in a real environment may have significant influence on the mechanical strength of concrete with MSWI ash. On the other hand, the curing temperature will also impact the leaching of heavy ions from WFA. However, little information concerning this has been reported [20].

Reactive powder concrete (RPC) was invented based on the maximum density theory [21–23]. This type of concrete, with high mechanical strength and durability, has been applied in a variety of construction applications [24]. Additionally, this kind of concrete is composed of large amounts of cementitious materials such as cement, silica fume, and blast furnace slag powder [25]. The addition of MSWI ash may partially replace cement and realize the recycling of waste.

In this study, the influence of solid waste incineration ash and curing temperatures on the mechanical strengths of RPC was investigated. The coupling effects of NaCl freeze–thaw erosion and carbonation were considered. The leaching amounts of cadmium and zinc were tested. The inner mechanism of the mechanical strengths of RPC with WFA has been reported in prior journals. However, this research provides a reference for the application of WFA in reactive powder concrete. Research and development of RPC with WFA is a new concept in the treatment of WFA. Meanwhile, research on the influence of the curing temperature and application environment on the properties of RPC will provide more application channels for the RPC with WFA.

2. Materials and Methods

2.1. Raw Materials

Ordinary Portland cement provided by Henan Dadi Cement Co., Ltd., Baofeng, China, was used in this study. The compressive strength, density, and the initial and final setting times of the cement used in this study were 42.5 MPa, 3.1 g/cm³, and 114 and 346 min, respectively. All technical performance indicators conformed to the GB175-2007 Chinese standard [26].

All of the granulated blast furnace slag powder (GGBS) and the superfine silica fume (SF), which were manufactured by Henan Zhongchuang Building Materials Co., Ltd., Zhengzhou, China, were used as mineral admixtures in the experiment. Additionally, the silica fume possessed a specific surface area of 15 m²/g and SiO₂ content higher than 98%. The silica fume showed a density of 2.2 g/cm³. The physical and chemical properties of silica fume were provided by the manufacturer of the silica fume. The density and the specific surface area of the GGBS were 2.9 g/cm³ and 436 m²/g, respectively. Furthermore, the loss on ignition of GGBS was 2.3%. The particle sizes of quartz sand used in this study were 1–0.71, 0.59–0.35, and 0.15–0.297 mm, and the mass ratios were 1:1.5:0.8. The quartz sand was composed of 99.6% SiO₂, 0.02% Fe₂O₃, and other ingredients. The mass ratio of quartz sand to binder materials was 1.25, and the mass ratio of cement:SF:GGBS was 1:0.5:0.15. The WFA applied in this research was provided by Jiangsu ouhang Environmental Protection Technology Co., Ltd., Kunshan, China. The mix proportion of reactive powder concrete was obtained based on the maximum density theory referred to in prior journals [27,28]. The mix proportion is shown in Table 1, which was obtained from previous research [29,30]. Polycarboxylate superplasticizer with water reducing rate of 40% manufactured by Henan Lichuang Lier Technology Co., Ltd., Pingdingshan, China, was applied in the adjustment of the fluidity of fresh reactive powder concrete. The dosage of polycarboxylate superplasticizer was 1.3% by the mass ratio of all binder materials. The water/binder ratio in this study was 0.2. The chemical composition and the particle passing percentage of raw materials are shown in Tables 2 and 3. A laser particle size analyzer was applied in the measurement of the particle size distribution. The testing results were provided by the manufactures.

Table 1. Mixture design of WFA-RPC per one cubic meter (kg).

Water	OPC	WFA	SF	GGBS	Quartz Sand	Water Reducer
244.4	740.7	0	370.3	111.1	977.9	16.3
244.4	679.6	61.1	370.3	111.1	977.9	16.3
244.4	618.5	122.2	370.3	111.1	977.9	16.3
244.4	557.4	183.3	370.3	111.1	977.9	16.3
244.4	496.3	244.4	370.3	111.1	977.9	16.3
244.4	435.2	305.5	370.3	111.1	977.9	16.3

Table 2. Chemical composition (wt.%) of the cementitious materials used in this study.

Types	SiO ₂	Al ₂ O ₃	Fe _x O _y	MgO	CaO	SO ₃	K ₂ O	Na ₂ O	Ti ₂ O	CdO	Cr ₂ O ₃	PbO	CuO	ZnO	Loss on Ignition
WFA	22.5	4.5	0.9	-	20.3	9.3	6.0	4.3	10.2	0.07	0.09	0.09	0.09	0.5	21.2
P·O cement	20.9	5.5	3.9	1.7	62.2	2.7	-	-	-	-	-	-	-	-	3.1
GGBS	34.1	14.7	0.2	9.7	35.9	0.2	3.5	-	-	-	-	-	-	-	-
Silica fume	90	0.2	0.6	0.2	0.4	0	7.4	-	-	-	-	-	-	-	-
Quartz sand	99.6	-	0.02	-	-	-	-	-	-	-	-	-	-	-	-

Table 3. Measured particle size distributions of the cementitious materials (%).

Types	Particle Size/ μm						
	0.3	0.6	1	4	8	64	360
WFA	0.13	0.5	2.2	17.2	31.3	97.5	100
P·O cement	0	0.3	2.7	15.0	28.8	93.6	100
GGBS	0.03	0.1	3.5	19.6	35.0	97.9	100
Silica fume	31.2	58.3	82.3	100	100	100	100
Quartz sand	0	0	0	0	0.03	20	100

2.2. Samples Preparation and Measurement Methods

The specimens of reactive powder concrete were prepared using the following steps.

The raw materials, including solid waste incineration ash and quartz sand, were mixed in the UJZ-15 mortar mixer for 30 s, and then the solution for the water-reducing agent mixture and water was added and mixed for 3.5 min. After mixing, fresh reactive powder concrete was applied for the measurement of slump flow. The specific experimental methods of the Nld-3 cement mortar fluidity tester, provided by Jianyi Zhongke Experimental Instrument Manufacturing Co., Ltd., were applied in the measurement of the slump flow of the reactive powder concrete. The specific testing procedures for the slump flow were carried out in reference to the Chinese standard GB/T 2419-2005 [31]. After stirring, the slump flow of fresh reactive powder concrete was determined and poured into molds in the sizes 40 × 40 × 160 mm; 100 × 100 × 100 mm; Φ 100 × 50 mm. The specimens were sealed with plastic cloth and kept in a room environment which had a temperature and relative humidity that were kept at 20 ± 2 °C and above 40%, respectively, for 1 day. After curing, the specimens were demolded and some of them were moved to the curing environment with a temperature of 20 ± 2 °C and a relative humidity of above 95% for the curing ages of 3, 7, 14, 21, 28, 60, 90, and 120 days. Several specimens were moved to a different environment (temperatures of 0, 20, and 40 °C with a relative humidity of above 95%) for 3, 28, and 90 days. The curing process is described in the GB/T50081 Chinese standard [32].

The YAW-300 microcomputer full-automatic universal tester, provided by Shanghai Qunhong Instrument Equipment Co., Ltd., Shanghai, China, was applied for the determination of the compressive strength and flexural strength. The sizes (40 × 40 × 160 mm) of the specimens for testing the mechanical strengths followed the GB/T 17671-1999 Chinese standard [33]. Figure 1 shows the test specimens and experimental setting pictures for measuring compressive strength and flexural strength.

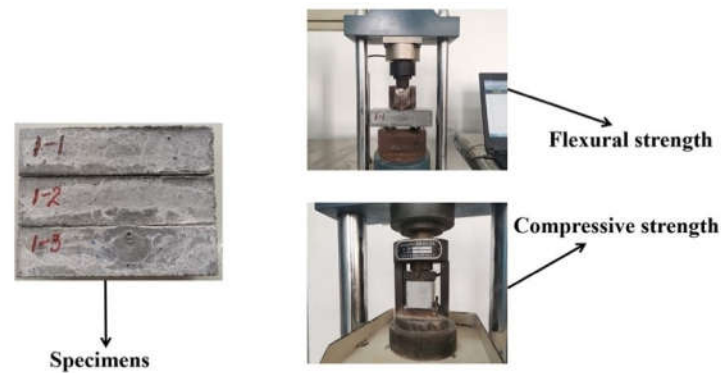


Figure 1. The flexural and compressive strengths of RPC with WFA.

Then, 3% NaCl solution was provided for the NaCl freeze–thaw cycles. The samples cured in a standard curing environment for 24 days were immersed in 3% NaCl solution for 4 days. All samples were then placed in the rapid freeze–thaw testing machine, and the NaCl freeze–thaw experiments were conducted. After different NaCl freeze–thaw cycles, the mass and mechanical strengths were tested, and the mass and mechanical strength losses were calculated. Additionally, some specimens after different NaCl freeze–thaw cycles were moved to a CCB-70F automatic concrete carbonation test box, produced by Hebei Shengxing Instrument Equipment Co., Ltd., (Cangzhou, China), and cured at a carbon dioxide concentration of 20% by the mass ratio of the total mass of gas and cured for 60 days before determination. Cylinder specimens with a size of $\Phi 100 \times 50$ mm were applied for the determination of chloride migration coefficient (CMC). The experiments of the NaCl freeze–thaw cycles and chloride migration coefficient were all conducted according to the Chinese GB/T 50082-2009 standard [34].

The leaching of the toxic metal ions can be determined according to the following steps. Specimens with size of $100 \times 100 \times 100$ mm and cured for 28 days were immersed in deionized water for 6 months. The leaching solution selected from the immersed deionized water per month was applied for the analysis of element content by an IRIS Intrepid ER/S ICP atomic emission spectrometer provided by the Thermo Elemental company, Waltham, Massachusetts, USA. Six specimens were provided in the experiment for each test. The testing process was carried out according to Reference [35].

3. Results and Discussion

3.1. The Flowability

Figure 2 shows the slump flow of fresh RPC with different dosages of WFA. As depicted in Figure 2, the slump flow of all fresh pastes decreased with an increase in the WFA dosage. The fluidity of fresh RPC depends on the inner free water [36]. It can be observed from Figure 2 that the error bar values were lower than 0.1, indicating that the accuracy of this experiment was high. Comparing the rheological properties of plain fresh RPC, the addition of WFA led to a decrease in the slump flow of the fresh paste. It can be obtained from Table 3 that the fineness of the WFA was higher than that of the cement. WFA with larger specific surface areas will exhibit higher water absorption than cement binders, which will lead to a reduced slump flow of RPC with an increasing content of WFA. In addition, the incorporation of WFA will decrease the setting time of the concrete. Both factors contribute to a reduced slump flow of RPC with WFA, which is consistent with our previous work in [37].

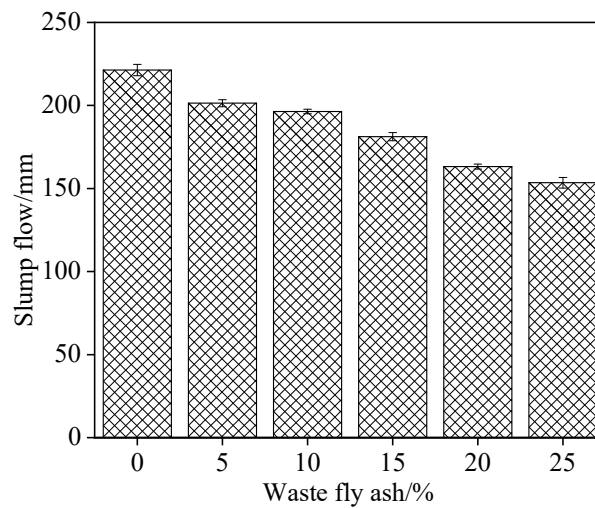


Figure 2. The slump flow of fresh RPC with WFA.

3.2. The Mechanical Strengths

Figure 3a,b show the flexural and compressive strengths of hardened RPC with WFA. The variation rates of the mechanical strengths by the addition of WFA were calculated and are shown in Figure 3c,d. The variation rate of the mechanical strength was calculated using Equation (1):

$$\Delta f = \frac{f_0 - f_m}{f_0} \quad (1)$$

where Δf represents for the variation rate of the flexural or compressive strengths; f_0 and f_m are the flexural or compressive strength of controlled RPC and RPC with WFA, respectively.

As shown in Figure 3, the flexural and compressive strengths at early curing ages (flexural strength: no more than 14 days; compressive strength: no more than 28 days) first exhibited an increasing and then a decreasing trend with the increase in the dosage of WFA. This was due to the fact that the addition of WFA with pozzolanic/hydraulic properties and high surface area can promote early-age hydration of cement-based materials, thus facilitating the strength development of RPC. As expected, the variations in the flexural strength measurements were higher when compared with compressive strengths. However, the dosage of WFA was higher than 10%, the mechanical strengths decreased by the increasing dosage of WFA due to the fact that WFA has a large specific surface area and many internal pores, thus reducing the mechanical properties [35,38,39]. Regarding the ratios of the mechanical property changes, it can be observed that although the early-age compression and flexural strengths' dependence on the dosage were not fully the same, the correlation between the long-term (after 28 days) properties and dosage showed good consistency for both the compressive and flexural strengths. For instance, both the flexural and compressive strengths of RPC cured for 120 days exhibited a monotonical decrease with the increase in the dosage of WFA, and both properties were reduced by approximately 25%, which is consistent with the literature [17]. From the above, the addition of WFA can both increase the compressive and flexural strengths at early-age hydration when the dosage is low (i.e., $\leq 10\%$); however, the long-term mechanical properties will always deteriorate with the addition of WFA at any dosage. This phenomenon may be explained by the fact that WFA, which has a smaller particle size and higher pozzolanic activity, might have a synergistic impact with cement hydration, resulting in improved

early-age mechanical properties. However, the chemical composition contains considerable amounts of alkalis and heavy metals, and the porous nature of WFA will deteriorate the long-term mechanical properties. These results provide necessary information on the mechanical properties when WFA is used as a cement replacement. Note that the error bars in Figure 3c,d can be deduced from Figure 3a,b; therefore, they are omitted here for clarity.

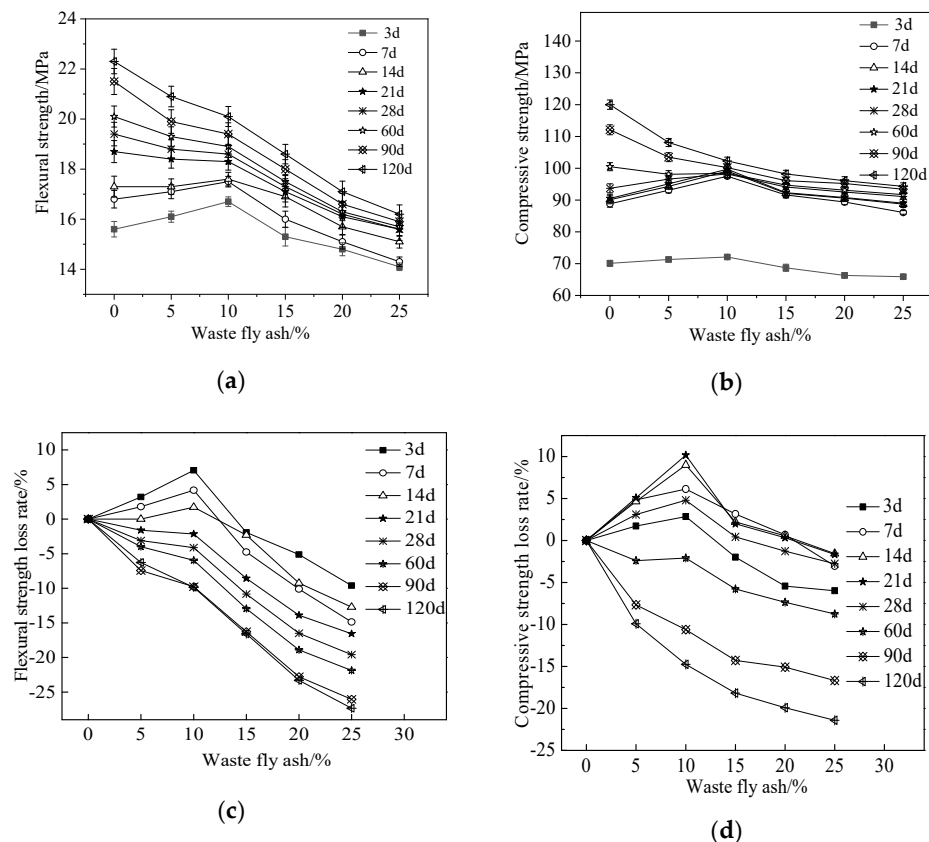


Figure 3. The mechanical strengths of RPC with WFA: (a) flexural strength; (b) compressive strength; (c) flexural strength loss rate; (d) compressive strength loss rate.

Figure 4a,b show the flexural and compressive strengths of RPC with WFA cured at temperatures of 0, 20, and 40 °C, respectively. Figure 4c,d show the increasing rates of the flexural and compressive strengths of RPC cured at temperatures of 20 and 40 °C compared with that of the RPC specimens cured at 0 °C. The curing ages were 3, 28, and 90 days, respectively. As shown in Figure 4, the mechanical strengths increased with an increase in the curing temperatures. This trend agrees well with the strength development of fly ash-based geopolymers [40]. Additionally, the increasing rates of the mechanical strengths of RPC at lower curing ages were higher than that at higher curing ages. This was due to the fact that the increased temperatures can accelerate the hydration reaction rate to improve the hydration degree of WFA RPC, thus improving the mechanical strengths [11,16,41]. However, with the continuous increase in the curing time, the degree of hydration tends to be stable. Therefore, the increasing rates of the mechanical strengths at later curing ages were lower than that at earlier curing ages. The low variations in Figure 4a,b indicate the good consistency of the experimental results. For clarity, the error bars in Figure 4c,d are omitted.

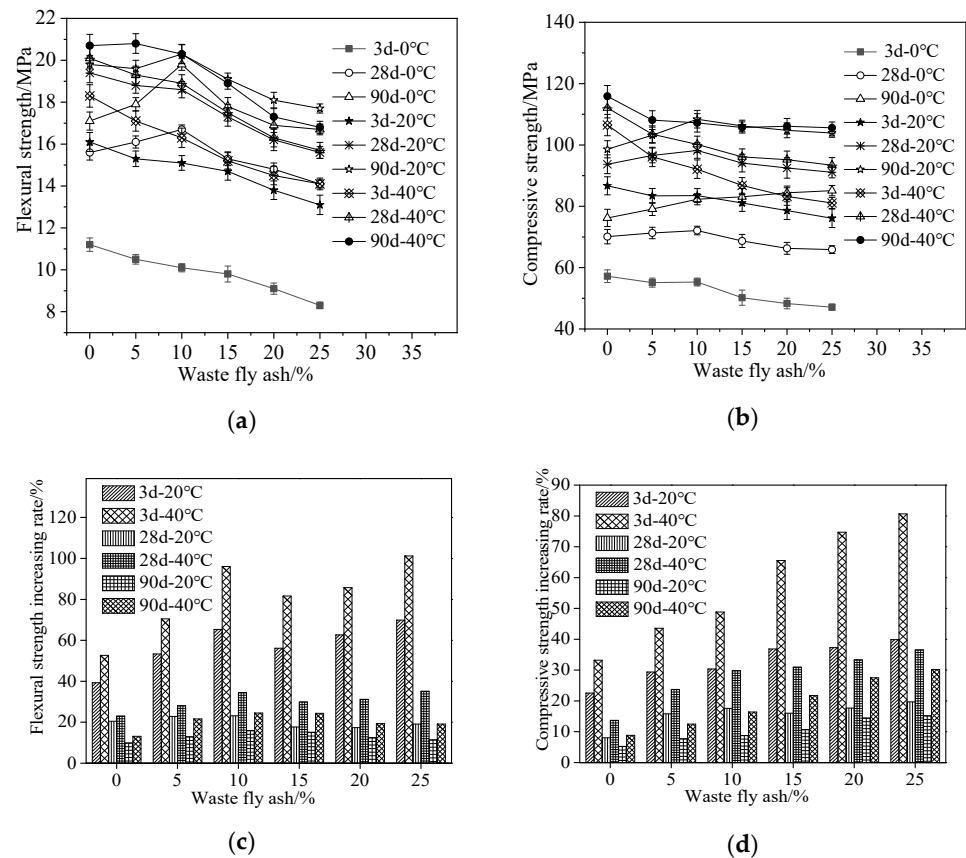


Figure 4. The mechanical strengths of RPC with WFA cured at different temperatures: (a) flexural strength; (b) compressive strength; (c) flexural strength loss rate; (d) compressive strength loss rate.

3.3. NaCl Freeze–Thaw Tests

Figure 5 demonstrates the mass loss rate of RPC with WFA during different NaCl freeze–thaw cycles. Table 3 shows the detailed parameters of the fitting between the mass loss rate and the NaCl freeze–thaw cycles (N) of RPC. a , b , and c were constants; meanwhile, R^2 was the fitting degree of the fitting curves. The mass loss rate rose noticeably as the number of NaCl freeze–thaw cycles increased as seen in Figure 5. This was due to the fact that using NaCl solution as a medium for the freeze–thaw cycles might exacerbate the fatigue effect [42,43]. Therefore, the external surface of concrete spalled due to the freeze–thaw actions. As observed from Figure 5, a significant decline in the mass loss rate occurred when the mass ratio of WFA ranged from 0% to 10%. However, when the dosage of WFA varied from 10% to 20%, a growth trend in the mass loss rate occurred. The correlation between the number of NaCl freeze–thaw cycles and the mass loss rate was fitted using a positive correlation quadratic function, with the fitting degrees exceeding 0.96 in all of the curves (shown in Table 4), indicating good correlations.

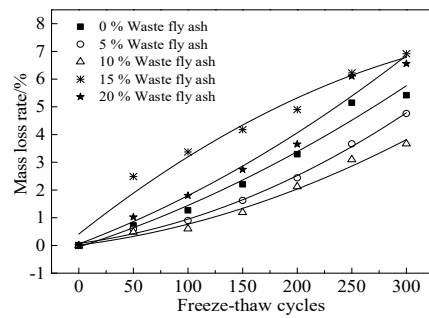


Figure 5. The measured mass loss rates of RPC with WFA during different NaCl freeze–thaw cycles.

Table 4. Relations between the mass loss rate and NaCl freeze–thaw cycles (*N*).

Equation	WFA Content/%	<i>a</i>	<i>b</i>	<i>c</i>	<i>R</i> ²
$\frac{\Delta m}{m} = aN^2 + bN + c$	0	2.19×10^{-5}	0.0128	−0.0550	0.967
	5	3.48×10^{-5}	0.00527	0.0751	0.996
	10	2.57×10^{-5}	0.00498	0.0139	0.980
	15	-3.31×10^{-5}	0.0312	0.411	0.964
	20	2.61×10^{-5}	0.0148	0.0553	0.967

Figure 6 shows the loss rate in the mechanical strengths of RPC with WFA at different NaCl freeze–thaw cycles. As demonstrated in Figure 6, the flexural and compressive strengths both decreased with an increasing number of NaCl freeze–thaw cycles. This was attributed to the fact that internal cracks are continuously induced by NaCl freeze–thaw cycles [44–46]. The flexural strength decreased at a rate of 0–10.63%. Meanwhile, the compressive strength showed a descending rate of 0–1.51%, indicating that the compressive strength presented a lower reduction. As depicted in Table 5, the relationship between mechanical strengths and the number of NaCl freeze–thaw cycles can be expressed through quadratic functions. Moreover, the mechanical strengths’ loss rate firstly decreased and then increased with an increasing dosage of WFA. When the content of WFA reached 10%, the mechanical strengths’ loss rates were the lowest.

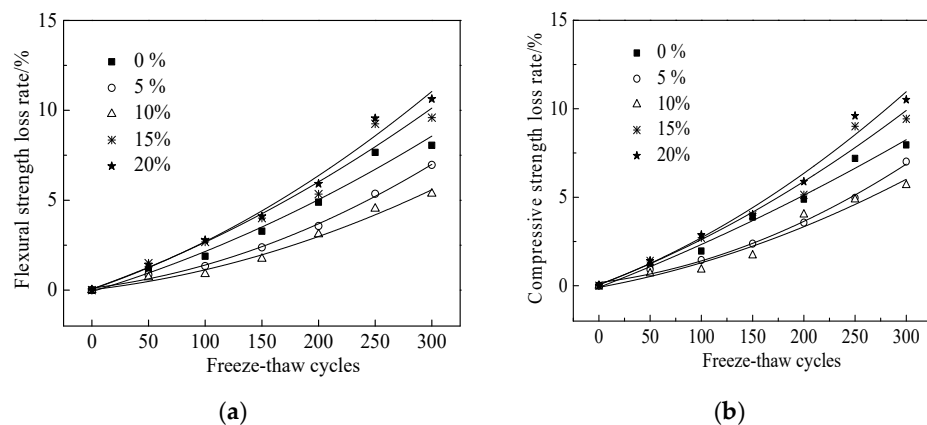


Figure 6. Relationship between the mechanical strength loss rates of RPC with WFA and NaCl freeze–thaw cycles: (a) flexural strength (*f_t*) loss rate; (b) compressive strength (*f_{cu}*) loss rate.

Table 5. Fitting parameters of mechanical strength loss rates and the number of NaCl freeze–thaw cycles (N).

Equation	WFA Content/%	a	b	c	R^2
$f_t = aN^2 + bN + c$	0	3.26×10^{-5}	0.0190	-0.0818	0.967
	25	5.05×10^{-5}	0.00778	0.113	0.996
	50	3.73×10^{-5}	0.00733	0.0223	0.980
	75	3.75×10^{-5}	0.02228	0.0631	0.955
	100	5.08×10^{-5}	0.0214	0.0502	0.977
$f_{cu} = aN^2 + bN + c$	0	1.78×10^{-5}	0.0225	-0.0946	0.983
	25	5.02×10^{-5}	0.00726	0.175	0.994
	50	3.23×10^{-5}	0.0107	-0.0941	0.945
	75	3.67×10^{-5}	0.0218	0.0595	0.955
	100	4.88×10^{-5}	0.0217	0.0522	0.972

Figure 7 shows the changes in the chloride migration coefficients of RPC with WFA during NaCl freeze–thaw cycles. As shown in Figure 7, the chloride migration coefficient continued to rise with an increase in the number of NaCl freeze–thaw cycles. This was due to the fact that the cracks induced by freeze–thaw cycles facilitate the migration of chloride ions, thus increasing the chloride migration coefficient of RPC with WFA [47]. Additionally, when the dosage of WFA ranged from 0% to 10%, the chloride migration coefficient decreased with the increasing dosage of WFA due to the promoting effect of WFA on the hydration of cement. This may be attributed to WFA which has a finer size that can effectively fill the inner pores of concrete. However, when the content of WFA increased from 10% to 20%, the increasing dosage of WFA led to an increasing chloride migration coefficient due to the lower flowability of concrete with excess WFA. We also noticed that the uncertainties in the CMC measurements became larger with an increase in the number of freeze–thaw cycles.

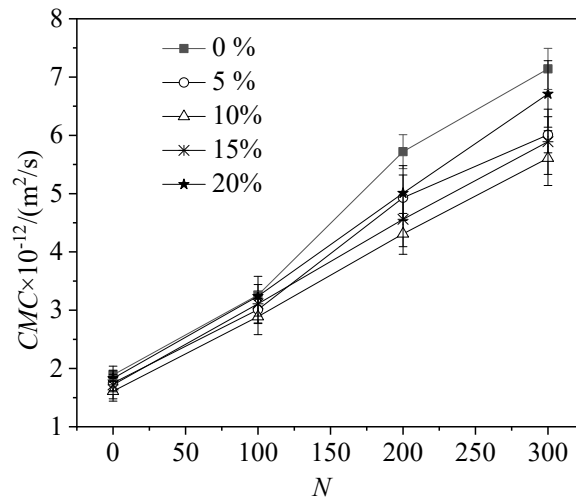
**Figure 7.** Evolution of chloride migration coefficients as a function of NaCl freeze–thaw cycles.

Figure 8 shows the carbonation depth of RPC with WFA during different NaCl freeze–thaw cycles. As demonstrated in Figure 8, the carbonation depth decreased obviously with increasing dosages of WFA. This was attributed to the fact that the WFA with alkalinity could absorb carbon dioxide, thus improving the carbonation resistance of RPC [48]. Moreover, as observed from Figure 8, the carbonation depth will increase with an increase in the freeze–thaw cycles, which can be attributed to the formation and propaga-

tion of microcracks inside concrete upon freeze–thaw damages. These microcracks facilitate the penetration of CO₂ inside concrete, which enabled more parts of the concrete to be exposed to carbon dioxide [49]. Owing to these factors, the carbonation depth kept increasing with the NaCl freeze–thaw cycles.

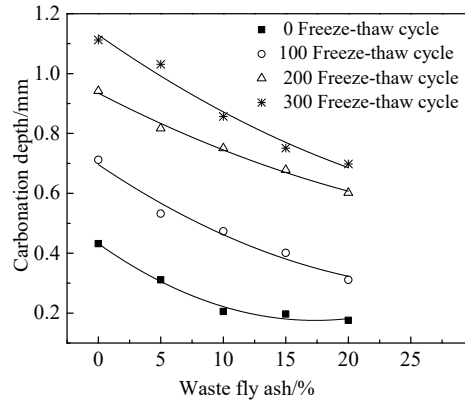
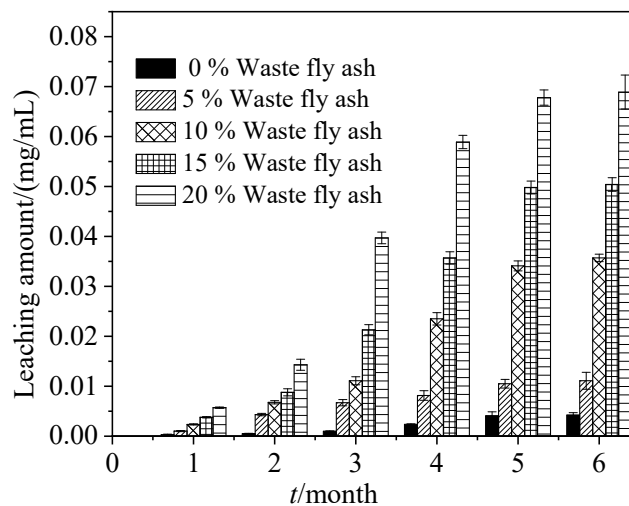


Figure 8. Carbonation depth of RPC with WFA at different NaCl freeze–thaw cycles.

Figure 9 shows the leaching amount of toxic metal elements. As depicted in Figure 9, the leaching amount of toxic metal elements first increased obviously when the leaching time increased from 0 to 5 months. However, when the leaching time increased from 5 to 6 months, the leaching amount of toxic metal elements tended toward stable values. Moreover, as observed in Figure 9, increasing dosages of WFA will lead to an increase in the leaching amount of toxic metal elements. Furthermore, the leaching amount of Cr is higher than the leaching amount of Zn. The largest variation in all of the leaching amounts was approximately 0.003 mg/mL, which indicates the good consistency of the leaching measurements.



(a)

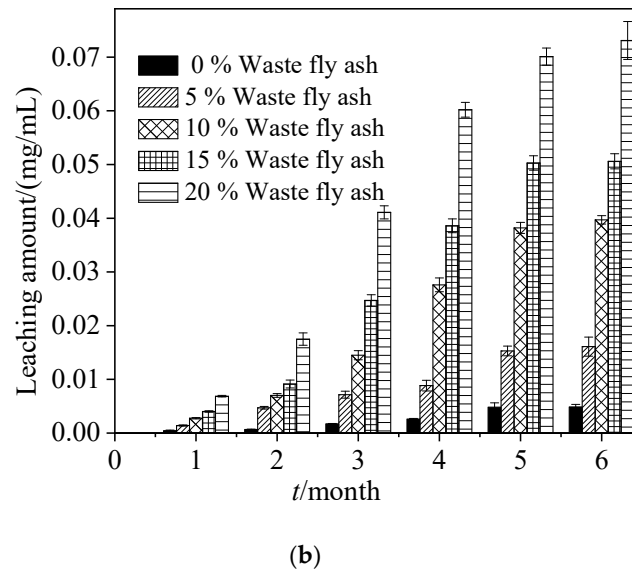
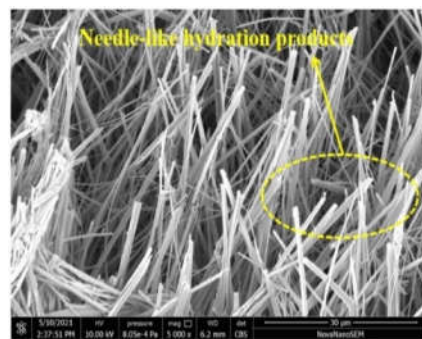
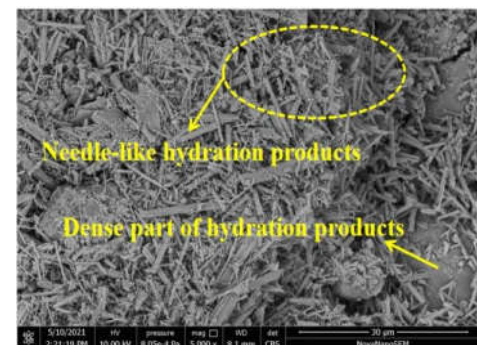


Figure 9. The leaching amount of toxic metal elements: (a) Cr; (b) Zn.

Scanning electron microscopy (SEM) was then adopted to investigate the influence of WFA on the microstructure of hydrated RPC. Figure 10 shows SEM images of RPC with 0% and 10% WFA cured in the standard curing condition and an environment of 40 °C and a 95% relative humidity. As shown in Figure 10a, a large number of acicular hydration products were observed in the specimen with 0% WFA after curing in the standard curing environment for 1 day. However, the fraction of needle-like products decreased, and the hydration products became more compact when 10% WFA was added into the RPC. Moreover, when cured at a higher curing temperature, the needle-like hydration products in specimens with 0% WFA gradually connected into a network of hydration products (shown in Figure 10c). As shown in Figure 10d, the addition of WFA could effectively increase the compactness of hydration products due to the improved hydration process by WFA. Figure 10e shows the control specimen cured for 28 days; it can be observed that the microstructure of RPC was compact and consisted of a large number of flocculent hydration products. Comparing Figure 10e and Figure 10f, the addition of WFA improved the compactness of the hydration products, which indicates that the WFA was beneficial to the microstructures of RPC with improved durability.



(a)



(b)

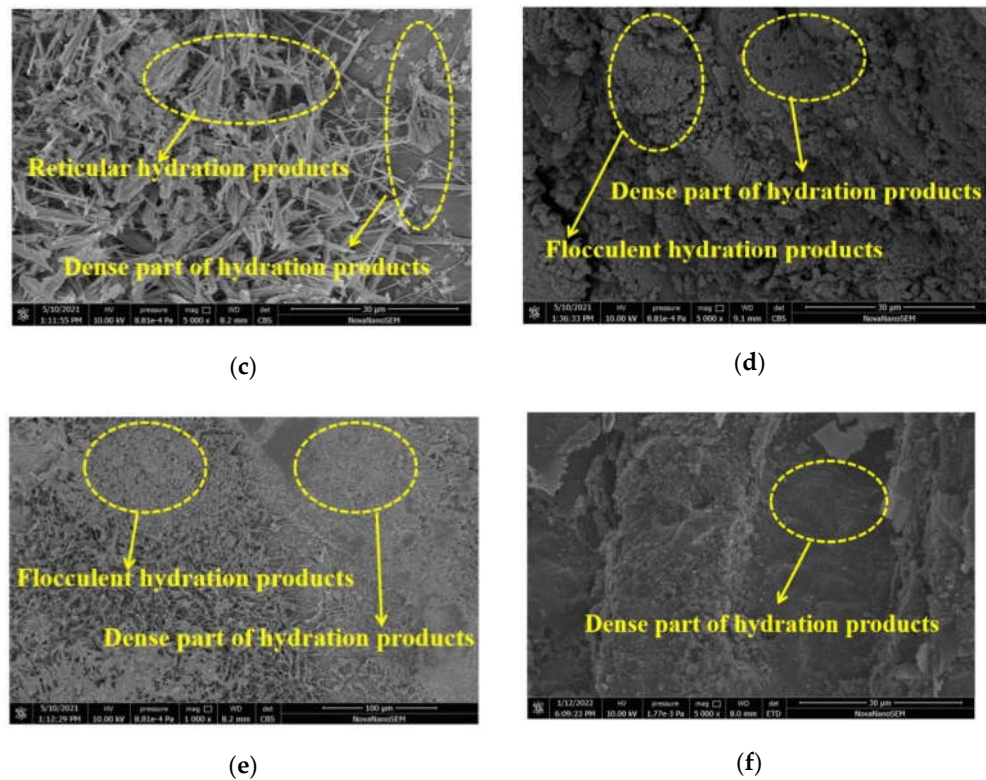


Figure 10. SEM microstructural images of RPC: (a) 0% WFA under standard curing for 1 day; (b) 10% WFA under standard curing for 1 day; (c) 0% WFA cured at 40 °C for 1 day; (d) 10% WFA cured at 40 °C for 1 day; (e) 0% WFA under standard curing for 28 days; (f) 10% WFA under standard curing for 28 days.

4. Conclusions

In this study, the mechanical strengths, resistances of NaCl freeze–thaw cycles, and the carbonation effect of RPC with WFA were systematically investigated. The following conclusions can be summarized.

Due to the relatively smaller particle size of WFA, the addition of WFA will reduce the flowability of fresh RPC. With a WFA content of $\leq 10\%$, the early-age strengths were increased by up to 10%. However, the long-term strengths of RPC were reduced by WFA; specifically, the mechanical strengths at 120 d were reduced by 25% with 25% WFA.

The NaCl freeze–thaw resistance of RPC can be optimized by adding 10% WFA, which results in a mass loss rate decrease of approximately 30% after 300 freeze–thaw cycles. Furthermore, the carbonation depth of RPC will decrease with an increase in the WFA content. The improved durability of RPC with WFA was found to be related to a refined microstructure from SEM observations.

The leaching amount of toxic metal elements showed an increasing trend with the increase in WFA content over the leaching time. The leaching amount of toxic metal elements reached a plateau at 5 months. The ultimate leaching amount of Cr slightly surpassed Zn, which was approximately 0.07 mg/mL.

Overall, our results demonstrated that RPC with up to 10% WFA still possessed comparable mechanical performance and durability to conventional RPC, which is a promising way to mitigate the environmental impact of WFA.

Author Contributions: Conceptualization, Y.D. and T.D.; methodology, Y.D.; validation, Y.D. and T.D.; formal analysis, Y.D., W.H., and H.W.; investigation, Y.D., W.H., S.W., and F.X.; resources, Y.D.; data curation, Y.D., and S.W.; writing—original draft preparation, Y.D. and H.W.; writing—

review and editing, T.D., F.S., H.W., and T.D.; visualization, F.S.; supervision, Y.D.; project administration, Y.D. and H.W.; funding acquisition, Y.D. and T.D. All authors have read and agreed to the published version of the manuscript.

Funding: This work was sponsored by the Zhejiang Provincial Natural Science Foundation (No. Y22E081344), the National Natural Science Foundation of China (No. 51808300 and 52108259), the Natural Science Foundation of Jiangsu Province (No. BK20200655), and the Shuangchuang Program of Jiangsu Province (No. JSSCBS20211195).

Data Availability Statement: The data used to support the findings of this study are available from the corresponding author upon request.

Conflicts of Interest: The authors declare that there are no conflicts of interest regarding the publication of this paper.

References

- Avila-López, U.; Almanza-Robles, J.M.; Escalante-García, J.I. Investigation of Novel Waste Glass and Limestone Binders Using Statistical Methods. *Constr. Build. Mater.* **2015**, *82*, 296–303. <https://doi.org/10.1016/j.conbuildmat.2015.02.085>.
- Chen, L.; Wang, Y.-S.; Wang, L.; Zhang, Y.; Li, J.; Tong, L.; Hu, Q.; Dai, J.-G.; Tsang, D.C.W. Stabilisation/Solidification of Municipal Solid Waste Incineration Fly Ash by Phosphate-Enhanced Calcium Aluminate Cement. *J. Hazard. Mater.* **2021**, *408*, 124404. <https://doi.org/10.1016/j.jhazmat.2020.124404>.
- Ivan Diaz-Loya, E.; Allouche, E.N.; Eklund, S.; Joshi, A.R.; Kupwade-Patil, K. Toxicity Mitigation and Solidification of Municipal Solid Waste Incinerator Fly Ash Using Alkaline Activated Coal Ash. *Waste Manag.* **2012**, *32*, 1521–1527. <https://doi.org/10.1016/j.wasman.2012.03.030>.
- Chandler, A.J.; Eighmy, T.T.; Hjelmar, O.; Kosson, D.S.; Sawell, S.E.; Vehlow, J.; Sloat, H.A.; van der Hartlén, J. *Municipal Solid Waste Incinerator Residues*; Elsevier: Amsterdam, The Netherlands, 1997; ISBN 978-0-08-053718-4.
- Adamu, M.; Mohammed, B.S.; Shafiq, N.; Liew, M.S. Durability Performance of High Volume Fly Ash Roller Compacted Concrete Pavement Containing Crumb Rubber and Nano Silica. *Int. J. Pavement Eng.* **2020**, *21*, 1437–1444. <https://doi.org/10.1080/10298436.2018.1547825>.
- Diliberto, C.; Meux, E.; Diliberto, S.; Garoux, L.; Marcadier, E.; Rizet, L.; Lecomte, A. A Zero-Waste Process for the Management of MSWI Fly Ashes: Production of Ordinary Portland Cement. *Environ. Technol.* **2020**, *41*, 1199–1208. <https://doi.org/10.1080/09593330.2018.1525434>.
- Aubert, J.E.; Husson, B.; Sarramone, N. Utilization of Municipal Solid Waste Incineration (MSWI) Fly Ash in Blended Cement: Part 1: Processing and Characterization of MSWI Fly Ash. *J. Hazard. Mater.* **2006**, *136*, 624–631. <https://doi.org/10.1016/j.jhazmat.2005.12.041>.
- Qiao, X.C.; Tyrer, M.; Poon, C.S.; Cheeseman, C.R. Novel Cementitious Materials Produced from Incinerator Bottom Ash. *Resour. Conserv. Recycl.* **2008**, *52*, 496–510. <https://doi.org/10.1016/j.resconrec.2007.06.003>.
- Aubert, J.E.; Husson, B.; Vaquier, A. Use of Municipal Solid Waste Incineration Fly Ash in Concrete. *Cem. Concr. Res.* **2004**, *34*, 957–963. <https://doi.org/10.1016/j.cemconres.2003.11.002>.
- Polettini, A.; Pomi, R.; Sirini, P.; Testa, F. Properties of Portland Cement—Stabilised MSWI Fly Ashes. *J. Hazard. Mater.* **2001**, *88*, 123–138. [https://doi.org/10.1016/S0304-3894\(01\)00292-8](https://doi.org/10.1016/S0304-3894(01)00292-8).
- Saikia, N.; Kato, S.; Kojima, T. Production of Cement Clinkers from Municipal Solid Waste Incineration (MSWI) Fly Ash. *Waste Manag.* **2007**, *27*, 1178–1189. <https://doi.org/10.1016/j.wasman.2006.06.004>.
- Kikuchi, R. Recycling of Municipal Solid Waste for Cement Production: Pilot-Scale Test for Transforming Incineration Ash of Solid Waste into Cement Clinker. *Resour. Conserv. Recycl.* **2001**, *31*, 137–147. [https://doi.org/10.1016/S0921-3449\(00\)00077-X](https://doi.org/10.1016/S0921-3449(00)00077-X).
- Li, X.-G.; Lv, Y.; Ma, B.-G.; Chen, Q.-B.; Yin, X.-B.; Jian, S.-W. Utilization of Municipal Solid Waste Incineration Bottom Ash in Blended Cement. *J. Clean. Prod.* **2012**, *32*, 96–100. <https://doi.org/10.1016/j.jclepro.2012.03.038>.
- Rehman, A.U.; Lee, S.-M.; Kim, J.-H. Use of Municipal Solid Waste Incineration Ash in 3D Printable Concrete. *Process Saf. Environ. Prot.* **2020**, *142*, 219–228. <https://doi.org/10.1016/j.psep.2020.06.018>.
- Alderete, N.M.; Joseph, A.M.; Van den Heede, P.; Matthys, S.; De Belie, N. Effective and Sustainable Use of Municipal Solid Waste Incineration Bottom Ash in Concrete Regarding Strength and Durability. *Resour. Conserv. Recycl.* **2021**, *167*, 105356. <https://doi.org/10.1016/j.resconrec.2020.105356>.
- Tang, P.; Florea, M.V.A.; Spiesz, P.; Brouwers, H.J.H. Application of Thermally Activated Municipal Solid Waste Incineration (MSWI) Bottom Ash Fines as Binder Substitute. *Cem. Concr. Compos.* **2016**, *70*, 194–205. <https://doi.org/10.1016/j.cemconcomp.2016.03.015>.
- Bertolini, L.; Carsana, M.; Cassago, D.; Quadrio Curzio, A.; Collepardi, M. MSWI Ashes as Mineral Additions in Concrete. *Cem. Concr. Res.* **2004**, *34*, 1899–1906. <https://doi.org/10.1016/j.cemconres.2004.02.001>.
- Shi, H.-S.; Kan, L.-L. Leaching Behavior of Heavy Metals from Municipal Solid Wastes Incineration (MSWI) Fly Ash Used in Concrete. *J. Hazard. Mater.* **2009**, *164*, 750–754. <https://doi.org/10.1016/j.jhazmat.2008.08.077>.
- Rémond, S.; Pimienta, P.; Bentz, D.P. Effects of the Incorporation of Municipal Solid Waste Incineration Fly Ash in Cement Pastes and Mortars: I. Experimental Study. *Cem. Concr. Res.* **2002**, *32*, 303–311. [https://doi.org/10.1016/S0008-8846\(01\)00674-3](https://doi.org/10.1016/S0008-8846(01)00674-3).

20. Luna Galiano, Y.; Fernández Pereira, C.; Vale, J. Stabilization/Solidification of a Municipal Solid Waste Incineration Residue Using Fly Ash-Based Geopolymers. *J. Hazard. Mater.* **2011**, *185*, 373–381. <https://doi.org/10.1016/j.jhazmat.2010.08.127>.
21. Mayhoub, O.A.; Nasr, E.-S.A.R.; Ali, Y.A.; Kohail, M. The Influence of Ingredients on the Properties of Reactive Powder Concrete: A Review. *Ain Shams Eng. J.* **2021**, *12*, 145–158. <https://doi.org/10.1016/j.asej.2020.07.016>.
22. Cai, Z.; Wang, H. Influence of NaCl Freeze–Thaw Cycles on the Mechanical Strength of Reactive Powder Concrete with the Assembly Unit of Sulphoaluminate Cement and Ordinary Portland Cement. *Coatings* **2021**, *11*, 1238. <https://doi.org/10.3390/coatings11101238>.
23. Sadrekarimi, A. Development of a Light Weight Reactive Powder Concrete. *J. Adv. Concr. Technol.* **2004**, *2*, 409–417. <https://doi.org/10.3151/jact.2.409>.
24. Yu, J.; Zhang, A.; Zhang, L.; Wang, Q.; Li, K.; Wang, H. Study on the Performance of Low Water-Binder Ratio Cement Mortar with Excavated Soil Exposed to NaCl Freeze-Thaw Environment. *Mater. Res. Express* **2021**, *8*, 095511. <https://doi.org/10.1088/2053-1591/ac27d1>.
25. Richard, P.; Cheyreyzy, M. Composition of Reactive Powder Concretes. *Cem. Concr. Res.* **1995**, *25*, 1501–1511. [https://doi.org/10.1016/0008-8846\(95\)00144-2](https://doi.org/10.1016/0008-8846(95)00144-2).
26. GB175-2007; Common Portland Cement. The State Bureau of Quality and Technical Supervision: Beijing, China, 2007.
27. Wang, H.; Shi, F.; Shen, J.; Zhang, A.; Zhang, L.; Huang, H.; Liu, J.; Jin, K.; Feng, L.; Tang, Z. Research on the Self-Sensing and Mechanical Properties of Aligned Stainless Steel Fiber-Reinforced Reactive Powder Concrete. *Cem. Concr. Compos.* **2021**, *119*, 104001. <https://doi.org/10.1016/j.cemconcomp.2021.104001>.
28. Wang, H.; Gao, X.; Liu, J.; Ren, M.; Lu, A. Multi-Functional Properties of Carbon Nanofiber Reinforced Reactive Powder Concrete. *Constr. Build. Mater.* **2018**, *187*, 699–707. <https://doi.org/10.1016/j.conbuildmat.2018.07.229>.
29. Cui, L.; Wang, H. Research on the Mechanical Strengths and the Following Corrosion Resistance of Inner Steel Bars of RPC with Rice Husk Ash and Waste Fly Ash. *Coatings* **2021**, *11*, 1480. <https://doi.org/10.3390/coatings11121480>.
30. Cui, L.; Wang, H. Influence of Waste Fly Ash on the Rheological Properties of Fresh Cement Paste and the Following Electrical Performances and Mechanical Strengths of Hardened Specimens. *Coatings* **2021**, *11*, 1558. <https://doi.org/10.3390/coatings11121558>.
31. GB/T 2419-2005; Test Methods for Fluidity of Cement Mortar. The State Bureau of Quality and Technical Supervision: Beijing, China, 2005.
32. GB/T50081-2019; Standard for Test Method of Concrete Physical and Mechanical Properties. The State Bureau of Quality and Technical Supervision: Beijing, China, 2019.
33. GB/T 17671-1999; Method of Testing Cements-Determination of Strength. The State Bureau of Quality and Technical Supervision: Beijing, China, 1999.
34. GB/T 50082-2009; Standard for Test Method of Long-Term Performance and Durability of Ordinary Concrete: Beijing, China, 2009.
35. El-eswed, B.I. Chemical Evaluation of Immobilization of Wastes Containing Pb, Cd, Cu and Zn in Alkali-Activated Materials: A Critical Review. *J. Environ. Chem. Eng.* **2020**, *8*, 104194. <https://doi.org/10.1016/j.jece.2020.104194>.
36. Huang, G.; Wang, H.; Shi, F. Coupling Effect of Salt Freeze-Thaw Cycles and Carbonation on the Mechanical Performance of Quick Hardening Sulphoaluminate Cement-Based Reactive Powder Concrete with Basalt Fibers. *Coatings* **2021**, *11*, 1142. <https://doi.org/10.3390/coatings11091142>.
37. Huang, H.; Gao, X.; Wang, H.; Ye, H. Influence of Rice Husk Ash on Strength and Permeability of Ultra-High Performance Concrete. *Constr. Build. Mater.* **2017**, *149*, 621–628. <https://doi.org/10.1016/j.conbuildmat.2017.05.155>.
38. Huang, G.; Yuan, L.; Ji, Y.; Liu, B.; Xu, Z. Cooperative Action and Compatibility between Portland Cement and MSWI Bottom Ash Alkali-Activated Double Gel System Materials. *Constr. Build. Mater.* **2019**, *209*, 445–453. <https://doi.org/10.1016/j.conbuildmat.2019.03.141>.
39. Ferraro, A.; Farina, I.; Race, M.; Colangelo, F.; Cioffi, R.; Fabbicino, M. Pre-Treatments of MSWI Fly-Ashes: A Comprehensive Review to Determine Optimal Conditions for Their Reuse and/or Environmentally Sustainable Disposal. *Rev. Environ. Sci. Bio-Technol.* **2019**, *18*, 453–471. <https://doi.org/10.1007/s11157-019-09504-1>.
40. Hwang, Y.-H.; Kim, D.-G.; Shin, H.-S. Mechanism Study of Nitrate Reduction by Nano Zero Valent Iron. *J. Hazard. Mater.* **2011**, *185*, 1513–1521. <https://doi.org/10.1016/j.jhazmat.2010.10.078>.
41. Kjeldsen, P.; Barlaz, M.A.; Rooker, A.P.; Baun, A.; Ledin, A.; Christensen, T.H. Present and Long-Term Composition of MSW Landfill Leachate: A Review. *Crit. Rev. Environ. Sci. Technol.* **2002**, *32*, 297–336. <https://doi.org/10.1080/10643380290813462>.
42. Ormellese, M.; Berra, M.; Bolzoni, F.; Pastore, T. Corrosion Inhibitors for Chlorides Induced Corrosion in Reinforced Concrete Structures. *Cem. Concr. Res.* **2006**, *36*, 536–547. <https://doi.org/10.1016/j.cemconres.2005.11.007>.
43. Hong, X.; Wang, H.; Shi, F. Influence of NaCl Freeze Thaw Cycles and Cyclic Loading on the Mechanical Performance and Permeability of Sulphoaluminate Cement Reactive Powder Concrete. *Coatings* **2020**, *10*, 1227. <https://doi.org/10.3390/coatings10121227>.
44. Wang, H.; Gao, X.; Liu, J. Effects of Salt Freeze-Thaw Cycles and Cyclic Loading on the Piezoresistive Properties of Carbon Nanofibers Mortar. *Constr. Build. Mater.* **2018**, *177*, 192–201. <https://doi.org/10.1016/j.conbuildmat.2018.05.103>.
45. Cai, G.; Zhao, J. Application of Sulphoaluminate Cement to Repair Deteriorated Concrete Members in Chloride Ion Rich Environment-A Basic Experimental Investigation of Durability Properties. *KSCE J. Civ. Eng.* **2016**, *20*, 2832–2841. <https://doi.org/10.1007/s12205-016-0130-4>.

46. Liu, R.; Jiang, L.; Xu, J.; Xiong, C.; Song, Z. Influence of Carbonation on Chloride-Induced Reinforcement Corrosion in Simulated Concrete Pore Solutions. *Constr. Build. Mater.* **2014**, *56*, 16–20. <https://doi.org/10.1016/j.conbuildmat.2014.01.030>.
47. Yoon, I.-S. Simple Approach to Calculate Chloride Diffusivity of Concrete Considering Carbonation. *Comput. Concr.* **2009**, *6*, 1–18. <https://doi.org/10.12989/cac.2009.6.1.001>.
48. Gartner, E.; Hirao, H. A Review of Alternative Approaches to the Reduction of CO₂ Emissions Associated with the Manufacture of the Binder Phase in Concrete. *Cem. Concr. Res.* **2015**, *78*, 126–142. <https://doi.org/10.1016/j.cemconres.2015.04.012>.
49. Wang, H.; Zhang, A.; Zhang, L.; Liu, J.; Han, Y.; Wang, J. Research on the Influence of Carbonation on the Content and State of Chloride Ions and the Following Corrosion Resistance of Steel Bars in Cement Paste. *Coatings* **2020**, *10*, 1071. <https://doi.org/10.3390/coatings10111071>.